

Physico-chemical properties of the new generation IV iron preparations ferumoxytol, iron isomaltoside 1000 and ferric carboxymaltose

Susann Neiser · Daniel Rentsch · Urs Dippon · Andreas Kappler · Peter G. Weidler · Jörg Göttlicher · Ralph Steininger · Maria Wilhelm · Michaela Braitsch · Felix Funk · Erik Philipp · Susanna Burckhardt

Received: 2 March 2015 / Accepted: 4 March 2015 / Published online: 24 March 2015
© Springer Science+Business Media New York 2015

Abstract The advantage of the new generation IV iron preparations ferric carboxymaltose (FCM), ferumoxytol (FMX), and iron isomaltoside 1000 (IIM) is that they can be administered in relatively high doses in a short period of time. We investigated the physico-chemical properties of these preparations and compared them with those of the older preparations iron sucrose (IS), sodium ferric gluconate (SFG), and low molecular weight iron dextran (LMWID). Mössbauer spectroscopy, X-ray diffraction, and Fe K-edge X-ray absorption near edge structure spectroscopy indicated akaganeite structures (β -FeOOH) for the cores of FCM, IIM and IS, and a maghemite (γ -Fe₂O₃) structure for that of FMX. Nuclear magnetic resonance studies confirmed the structure of the carbohydrate of FMX as a reduced, carboxymethylated, low molecular weight

dextran, and that of IIM as a reduced Dextran 1000. Polarography yielded significantly different fingerprints of the investigated compounds. Reductive degradation kinetics of FMX was faster than that of FCM and IIM, which is in contrast to the high stability of FMX towards acid degradation. The labile iron content, i.e. the amount of iron that is only weakly bound in the polynuclear iron core, was assessed by a qualitative test that confirmed decreasing labile iron contents in the order $SFG \approx IS > LMWID \geq FMX \approx IIM \approx FCM$. The presented data are a step forward in the characterization of these non-biological complex drugs, which is a prerequisite to understand their cellular uptake mechanisms and the relationship between the structure and physiological safety as well as efficacy of these complexes.

Electronic supplementary material The online version of this article (doi:10.1007/s10534-015-9845-9) contains supplementary material, which is available to authorized users.

S. Neiser · M. Wilhelm · M. Braitsch · F. Funk · E. Philipp · S. Burckhardt (✉)
Chemical and Preclinical Research and Development,
Vifor (International) Ltd., St. Gallen, Switzerland
e-mail: susanna.burckhardt@viforpharma.com

D. Rentsch
Swiss Federal Laboratories for Materials Science and
Technology (Empa), Dübendorf, Switzerland

U. Dippon · A. Kappler
Geomicrobiology, Center for Applied Geosciences,
University of Tübingen, Tübingen, Germany

P. G. Weidler
Institute of Functional Interfaces, Karlsruhe Institute of
Technology (KIT), Eggenstein-Leopoldshafen, Germany

J. Göttlicher · R. Steininger
ANKA–Synchrotron Radiation Facility, Karlsruhe
Institute for Technology (KIT),
Eggenstein-Leopoldshafen, Germany

Keywords Intravenous iron · Iron sucrose · Ferric carboxymaltose · Iron isomaltoside 1000 · Ferumoxytol · Low molecular weight iron dextran

Abbreviations

DQF-COSY	Double quantum filtered correlation spectroscopy
EDTA	Ethylenediaminetetraacetic acid
FCM	Ferric carboxymaltose
FDA	U.S. Food and Drug Administration
FMX	Ferumoxytol
GFC	Gel-filtration chromatography
Glc	Glucose
GOF	Goodness of fit
HMBC	Heteronuclear multiple-bond correlation
HMWID	High molecular weight iron dextran
HSQC	Heteronuclear single quantum correlation
IIM	Iron isomaltoside 1000
IS	Iron sucrose
ISS	Iron sucrose similar
IV	Intravenous
LMWID	Low molecular weight iron dextran
M_n	Number average molecular weight
M_w	Weight average molecular weight
M_z	z-average molecular weight
NBCD	Non-biological complex drugs
NMR	Nuclear magnetic resonance
NTBI	Non-transferrin bound iron
P	Polydispersity
PSC	Polyglucose sorbitol carboxymethylether
QS	Quadrupole splitting
s	Standard deviation
SAED	Selected area electron diffraction
SD _{CM}	Carboxymethylation substitution degree
SFG	Sodium ferric gluconate
SHE	Standard hydrogen electrode
TEM	Transmission electron microscopy
TOCSY	Total correlation spectroscopy
TRIS	Tris(hydroxymethyl)aminomethane
USP	United States Pharmacopeia
XANES	X-ray absorption near edge structure
XRD	X-ray diffraction

Introduction

Intravenous (IV) iron therapy is widely used to treat iron deficiency and iron deficiency anemia (Auerbach and Ballard 2010). The indications include absolute iron deficiency, when there is a need for fast iron repletion or an intolerance to oral iron, as well as the therapy of anemia of chronic disease (ACD, also called iron sequestration syndromes) or functional iron deficiency (Goodnough et al. 2010). Under inflammatory conditions (anemia of chronic disease) or when there is a high iron demand for erythropoiesis (functional iron deficiency), such as during therapy with erythropoiesis stimulating agents, oral iron therapy is not effective and IV iron is recommended (Goodnough et al. 2010; Qunibi 2010). Therefore, the therapeutic areas for IV iron are widespread and, among others, include nephrology (Besarab and Coyne 2010; Macdougall et al. 2012), cardiology (Avni et al. 2012; Macdougall et al. 2012; von Haehling et al. 2012), oncology (Gafer-Gvili et al. 2013), gastroenterology (Gomollon and Gisbert 2013), and gynecology (Breyman et al. 2010; Haththotuwa et al. 2011), as well as patient blood management (pre-/postoperative anemia) (Shander et al. 2012).

All iron compounds used for IV iron therapy consist of a polynuclear Fe(III)-oxyhydroxide/oxide core surrounded by carbohydrates which stabilize the core and protect the nanoparticles against further polymerization (Auerbach and Ballard 2010; Kästele et al. 2014; Macdougall and Geisser 2013; Qunibi 2010). Despite their similar structure, IV iron compounds have distinct properties. In particular, they display a wide range of stability and, depending on the type of stabilizing carbohydrate, may have antigenic potential (Chertow et al. 2006). IV iron compounds belong to the class of so-called non-biological complex drugs (NBCD) which, in contrast to small molecules, cannot be fully characterised by physico-chemical methods and which are largely defined by the manufacturing process (Crommelin et al. 2014).

A main goal of the recent developments in the field of IV iron therapy was to provide a preparation that can be administered in higher doses and in a short period of time. Some of the older products, such as sodium ferric gluconate (SFG) and iron sucrose (IS) are not very stable and thus contain a higher percentage of labile, weakly-bound iron (Van Wyck et al.

2004; Van Wyck 2004). This property, together with the high osmolarity and the high pH of the solutions, limits the maximum single doses allowed for SFG and IS to 62.5–125 and 200–500 mg iron (Fe), respectively (Macdougall and Geisser 2013). In contrast, the three recently introduced IV iron preparations Ferinject®/Injectafer® (active ingredient: ferric carboxymaltose, FCM), Feraheme®/Rienso® (active ingredient: ferumoxytol, FMX), and MonoFer® (active ingredient: iron isomaltoside 1000, IIM), are more stable and can all be administered in comparatively high single doses (from 510 up to more than 1000 mg Fe) (Macdougall and Geisser 2013). An overview on selected properties and recommended dose regimen of the different preparations is given in Table 1.

FCM consists of a polynuclear Fe(III)-oxyhydroxide core surrounded by carboxymaltose which is derived from maltodextrin, an oligosaccharide produced from starch. IIM contains a polynuclear Fe(III)-oxyhydroxide core which is stabilized by a hydrogenated (reduced) Dextran 1000 (isomaltoside 1000) and a low amount of citrate (Andreasen and Christensen 2001; Medice Pharma GmbH&Co. KG, Iserlohn, Germany 2011; Nordfjeld et al. 2012; Pharmacosmos A/S, Holbaek, Denmark 2009). A different, matrix-like structure has been proposed for IIM (Jahn et al. 2011), but has recently been shown to be based on an incorrect interpretation of nuclear magnetic resonance (NMR) data (Kästele et al. 2014). FMX was originally developed as a contrast agent for magnetic resonance imaging and has been described as a superparamagnetic ferric oxide coated with polyglucose sorbitol carboxymethylether (PSC), a reduced and carboxymethylated dextran (Simon et al. 2006). FMX contains mannitol and further PSC as excipients (AMAG Pharmaceuticals Inc., Waltham, MA, USA 2009; European Medicines Agency 2012).

In this work, the physico-chemical properties of these three new preparations for parenteral iron therapy were characterized and compared. In particular, we show that despite the similarity of the investigated compounds, they show unique properties and important differences which may have an implication for their therapeutic application. Comparable techniques have been used previously to characterize some of these compounds, but direct comparison is not always available and there is not always a good agreement among the results (Balakrishnan et al. 2009; Funk et al. 2001; Fütterer et al. 2013; Jahn et al. 2011; Kudasheva et al. 2004).

Table 1 Chemical classification, dosing, and terminal half-life of the most important current IV iron preparations

Brand names	Ferrlecit®	CosmoFer®, INFeD®	Venofer®	Ferinject®, Injectafer®	MonoFer®	Feraheme®, Rienso®
Active ingredient	Sodium ferric gluconate (SFG)	Low molecular weight iron dextran (LMWID)	Iron sucrose (IS)	Ferric carboxymaltose (FCM)	Iron isomaltoside 1000 ^a (IIM)	Ferumoxytol (FMX)
Carbohydrate	Gluconate	Dextran	Sucrose	Carboxymaltose	Isomaltoside 1000 ^a	PSC ^b
Max. single Fe dose (min. admin. time) ^c	125 mg (10–60 min)	20 mg/kg b.w. (4–6 h)	200 mg (10–30 min)	1000 mg (15 min)	20 mg/kg b.w. (60 min)	510 mg (17 s)
Terminal half-life (dose in mg Fe) ^d	1.42 h (125)	27–30 h (500–2,000)	5.3 h (100)	7.4/9.4 h (100/1000)	20.8/22.5 h (100/200) ^e	14.7 h (316)

b.w. body weight

^a In German SPC (Medice Pharma GmbH&Co. KG, Iserlohn, Germany 2011): Iron citrate isomalto-oligosaccharide alcohol-hydrate complex

^b PSC, polyglucose sorbitol carboxymethylether

^c Most common maximal dose and corresponding minimal administration time: the exact posology may vary between markets. Please refer to local prescribing information

^d Geisser and Burckhardt (2011) and references cited therein

^e Nordfjeld et al. (2012)

Materials and methods

Materials

The following IV iron preparations were obtained from a pharmacy or directly from the manufacturer: Feraheme[®] (30 mg Fe/mL, AMAG Pharmaceuticals, Inc., Lexington, MA) and Rienso[®] (Takeda Global Research and Development Centre (Europe) Ltd., Aldwych-London, UK), active ingredient ferumoxytol (FMX); MonoFer[®] (100 mg Fe/mL, Pharmacosmos A/S, Holbaek, Denmark), active ingredient iron isomaltoside 1000 (IIM); Ferinject[®] (50 mg Fe/mL, Vifor (International) Ltd., St. Gallen, Switzerland), active ingredient ferric carboxymaltose (FCM); Venofer[®] (20 mg Fe/mL, Vifor (International) Ltd., St. Gallen, Switzerland), active ingredient iron sucrose (IS); Cosmofer[®] (50 mg Fe/mL, TEVA GmbH, Radebeul, Germany), active ingredient iron dextran, and Ferlecit[®] (12.5 mg Fe/mL, Sanofi-Aventis Deutschland GmbH, Frankfurt am Main, Germany), active ingredient sodium ferric gluconate (SFG). Since different lots were used, the lot numbers are indicated for each method separately.

Separation of mannitol from the FMX solution

To remove mannitol, 18 mL FMX solution (Feraheme[®] lot 09060402) were diluted with 7.2 mL distilled water and filtered with an Amicon Ultra-15 centrifugal filter device (IVD ultracel-10 K regenerated cellulose, molecular weight cut-off 10 kDa, Millipore, Ireland). The retentate was taken up six times with distilled water and centrifuged. The final retentate contained the mannitol-free FMX. Although the weight-average molecular weight of the carboxymethylated dextran in FMX is above the molecular weight cut-off of the filter, low-molecular weight fractions of the unbound carboxymethylated dextran may also have been partly removed from the solution by this method. The resulting material was used for X-ray diffraction (XRD) measurements and as starting material for the isolation of the FMX carbohydrate.

Isolation of the carbohydrates from the FMX and IIM solutions

The iron-carbohydrate nanoparticles were destroyed by heat treatment of the mannitol-free FMX (see section

above) and IIM (MonoFer[®] lot 949171-1) solutions in phosphate buffer: Product solution corresponding to 120 mg iron was mixed with 50 mL phosphate buffer (4.43 g KH₂PO₄/0.143 g Na₂HPO₄ per 500 mL) and heat treated at 132 °C and pH 5.4 for 90 min. The iron phosphate precipitate was separated from the carbohydrate-containing supernatant by centrifugation (10 min at 500 U/min). The heat treatment and centrifugation was repeated with the supernatant (132 °C, 15 min for FMX and 132 °C, 90 min for IIM). The filtrate of the supernatant was lyophilized and dissolved in distilled water [1.17 % (m/m)]. The resulting carbohydrate-containing solution from FMX was dialyzed with a regenerated, ethylenediaminetetraacetic acid (EDTA)-treated cellulose membrane (nominal cut-off 1000 Da, V-series by ZelluTrans Roth, Karlsruhe, Germany, lot 190119) to remove phosphate and again lyophilized. The lyophilisate from FMX most likely contains both the core-stabilizing PSC and PSC added as an excipient. Due to the lower molecular weight of isomaltoside 1000, the carbohydrate-containing solution from IIM was not purified by dialysis but by ion exchange (Merck ion exchanger V, no. 104836. Lot L701436 101) to remove the phosphate.

Mössbauer spectroscopy

An aliquot of 400 µL (FMX and IIM) or 450 µL (FCM) of liquid sample material was pipetted under oxic conditions into a Teflon sample container, sealed with Kapton tape and frozen at −30 °C. The frozen samples were transferred into a closed cycle helium cryostat and Mössbauer spectra were recorded at temperatures between 245 and 5 K. The Mössbauer spectra were recorded in transmission geometry using a constant acceleration drive system equipped with a ⁵⁷Co source in rhodium matrix and a proportional counter coupled to a CMCA-550 1024 multichannel analyzer (WissEL, Germany). All spectra were calibrated against a room temperature spectrum of a 7 µm alpha-Fe foil. The spectra were fitted using Voigt based spectral lines (RECOIL software suite, University of Ottawa, Canada). During fitting, the half-width-half-maximum of the peaks was kept at 0.097 mm/s and the Gauss sigma parameter was varied to account for line broadening. The blocking temperature was defined as the temperature at which 50 % of the material was paramagnetic and 50 % magnetically ordered (Funk et al. 2001; Murad 1996).

The following lots were analyzed: MonoFer[®] lot 949171-1, Feraheme[®] lot 09060402, Ferinject[®] lot 062201.

Iron(II) quantification

The amount of Fe(II) was determined by cerimetric titration with cerium sulfate and potentiometric end-point determination (Jander et al. 2003). The following lots were analyzed: MonoFer[®] lot 949171-1, Feraheme[®] lot 09060402, and 9 consecutive lots of Ferinject[®].

X-ray diffraction (XRD)

The samples were measured on different instruments (Bruker, Karlsruhe, Germany) as indicated in the Supplementary data (Table S1). All samples were transferred to a flat disk sample holder with a 1 mm deep round indentation with 20 mm in diameter. α -Al₂O₃ (corundum) was applied as an internal standard to all samples. Liquid samples were applied onto a Si single-crystal chip (diameter 1 inch) and air-dried at 50 °C.

The diffractograms were analyzed with the softwares DiffracPlus EVA 15.0 for a first identification of the crystalline phases, and TOPAS 4-2 (both Bruker AXS GmbH, Karlsruhe, Germany) for a more advanced determination of lattice constants by the Pawley method (Pawley 1981). Space group information was obtained from literature. The profile function applied to all refinements was a modified Thompson-Cox-Hastings pseudo-Voigt function (Young 1993). The goodness of fit parameter (GOF) was also calculated. A GOF of 1.0 corresponds to a perfect agreement between model and data. The domain size was determined from the Scherrer equation (Klug and Alexander 1974) and consideration of the instrumental contribution to line broadening determined from LaB₆ measurements.

X-ray absorption near edge structure spectroscopy (XANES)

Fe K-edge XANES spectroscopy was performed at the X-ray beamline of the Synchrotron Radiation Laboratory for Environmental Studies (SUL-X) of ANKA (Karlsruhe Institute for Technology, Eggenstein-Leopoldshafen, Germany) using a Si(111) crystal pair in a fixed exit monochromator. To avoid radiation damage the beam was collimated. Pellets of fine

grained goethite (α -FeOOH), lepidocrocite (γ -FeOOH), 2-line and 6-line ferrihydrite, as well as akaganeite (β -FeOOH) were prepared with cellulose in order to achieve optimal absorption for the spectra that were used as references. The liquid sample solutions (MonoFer[®] lot 224121-3; Venofer[®] lot 076201) were measured in a custom-made cell for liquid samples. The cell mainly consists of two Kapton-foils with an effective diameter of 10 and 0.7 mm separation, which results in a volume of 0.55 mm³. The foils are sealed with O-rings, and the parts are kept together by a metallic frame equipped with in- and outlets. The 0.7 mm spacing has been chosen because at that distance the transmission signal is not disturbed by the undiluted sample solution. Two cell fillings of each substance were measured, and each measurement was performed twice at the same spot to detect instrumental influences or changes within the sample that may occur due to high photon flux density. Energy step width across the edge was 0.3 eV. The energy has been calibrated to 7112 eV at the first maximum of the first derivative of a XANES spectrum of elemental Fe (Fe foil). All measurements were done in transmission mode using ionization chambers as detectors for the incident and absorbed beams of sample, reference substances and Fe foil. Spectra were added and averaged. Their pre- and post-edge ranges were approximated by linear and polynomial fit-functions. The edge jump was normalized to 1 in order to compare spectra with each other. Both steps of data processing were done with the Athena program of the IFEFFIT package (RAVEL and Newville 2005). Combinatorial Linear Combination Fits (LCF) have been performed with the Athena program of the IFEFFIT package for the Fe K-edge XANES spectra with five reference spectra: akaganeite, goethite, lepidocrocite, 2L-ferrihydrite (2L-Fh) and 6L-ferrihydrite (6L-Fh) (RAVEL and Newville 2005).

NMR spectroscopy

The ¹H and ¹³C NMR spectra of the IIM and FMX carbohydrates were recorded at 400.13 and 100.61 MHz on a Bruker Avance 400 NMR spectrometer (Bruker Biospin AG, Fällanden, Switzerland). The ¹H, the 1D diffusion-edited ¹H, and the ¹³C NMR spectra, as well as the ¹H-¹³C HSQC, ¹H-¹³C HMBC, ¹H-¹³C HSQC-TOCSY, and ¹H-¹H DQF-COSY 2D correlation NMR experiments were performed at 298 K on a 5 mm

broadband inverse probe equipped with z-gradient (100 % gradient strength of 53.5 Gcm^{-1}) applying 90° pulse lengths of $6.8 \mu\text{s}$ (^1H) and $14.5 \mu\text{s}$ (^{13}C). All NMR experiments were performed in D_2O solutions ($c = 50\text{--}200 \text{ mg/mL}$) using the Bruker standard pulse programs and parameter sets selecting coupling constants of 145 Hz (HSQC), 10 Hz (HMBC) and mixing times of 150 ms (HSQC-TOCSY). The ^1H and ^{13}C chemical shifts were externally referenced relative to the signals of 3-trimethylsilyl-2,2,3,3-tetra-deutero sodium propionate dissolved in D_2O at 0.0 and -1.6 ppm , respectively. The carbohydrates of following lots were analyzed: MonoFer[®] lot 949171-1, Feraheme[®] lot 09060402 and lot 10012802; Dextran 3–4000 (Amersham Biosciences, lot 303820) and Dextran 1000 (Sigma-Aldrich Switzerland, Lot BCBD4347V-02-002) were used as reference samples.

Molecular weight distribution

The molecular weight distribution was determined by gel-filtration chromatography (GFC) as described earlier (Geisser et al. 1992). The lot numbers of the investigated samples are given in the results section. For the determination of the molecular weight of carbohydrate samples, glucose and Dextran 1000 were used in addition to the pullulans P5, P10, and P20 as calibration standards (Geisser et al. 1992).

Polarographic analysis

The reduction potentials were measured by differential pulse polarography based on the US Pharmacopeia (USP) method described in the monograph for iron sucrose injection (U.S. Food and Drug Administration 2012b). The measurements were done at pH 7 in 15 % m/v acetate buffered solutions on a Metrohm 797 VA Computrace polarograph (Metrohm AG, Herisau, Switzerland) with a multi-mode working electrode, reference electrode $\text{Ag/AgCl}/c(\text{KCl}) = 1 \text{ mol/L}$, and with a platinum auxiliary electrode. The values reported in this work have been corrected by $+236 \text{ mV}$ to express the potentials relative to the standard hydrogen electrode (SHE). The iron concentrations in the sample solutions were 15, 50, 20, and $25 \mu\text{g/mL}$ for FMX, IIM, IS, and FCM, respectively. All iron formulations were measured immediately after opening the container. The following lots were analyzed: Feraheme[®] lot 10061002,

MonoFer[®] lot 042838-3, Venofer[®] lot 901201, Ferinject[®] lot 169001.

Reductive degradation kinetics

The reductive degradation kinetics were measured at pH 2.50–2.60 and 25°C in solutions containing ascorbic acid, citric acid, H_3PO_4 , Na_2HPO_4 (all 0.08 M), FeSO_4 (0.008 M), and sorbitol (1 M) (Erni et al. 1984). The analyzed lots are given in the results section.

“Tea test”

The “tea test” was used as a qualitative assay to visualize the content of labile, weakly-bound iron by reaction with polyphenols. Five bags of Lipton white tea (lot L23320D023; exp 11/2014. Unilever Schweiz, 8240 Thayingen, Switzerland) were placed in 2 L of a 0.9 % NaCl solution at $90\text{--}100^\circ\text{C}$ and allowed to steep for 1 min. White tea was chosen because of its light color combined with a high content of polyphenols. After the infusion had cooled to $<37^\circ\text{C}$, the iron preparations were added to result in an iron concentration of 0.1 mg/mL and stirred (Ferinject[®] lot 258001; MonoFer[®] lot 042838-3; Feraheme[®] lot A56996A; Venofer[®] lot 133001; Cosmofer[®] lot 1226801-3; Ferrlecit[®] lot D2A046A). No pH adjustment was done. The solutions were filled into cuvettes, and photographs were taken 1–2 h after sample preparation had started.

Results and discussion

Characterization of the polynuclear iron oxide/hydroxide cores

Mössbauer spectroscopy

The Mössbauer spectra of FMX could be modeled with parameters characteristic for Fe(III), with no indication of the presence of Fe(II). Based on hyperfine field parameters of the 5 K spectrum, FMX was identified as nano-maghemite (Fig. 1; Table 2) (Tronc et al. 2000; Tucek et al. 2006). The transition from the superparamagnetic to the magnetically-ordered state spanned a wide temperature range of more than 100 K. While the material is completely magnetically ordered at 5 K, first signs of magnetic relaxation were detected

Fig. 1 Mössbauer spectra of FMX, IIM and FCM recorded at 77 K (*left*) and 5 K (*right*). Colored dots represent the Mössbauer signal, dark grey lines the fit, and light gray lines the single models used for fitting of the spectra. Modeling parameters are given in Table S2 (Supplementary data). (Color figure online)

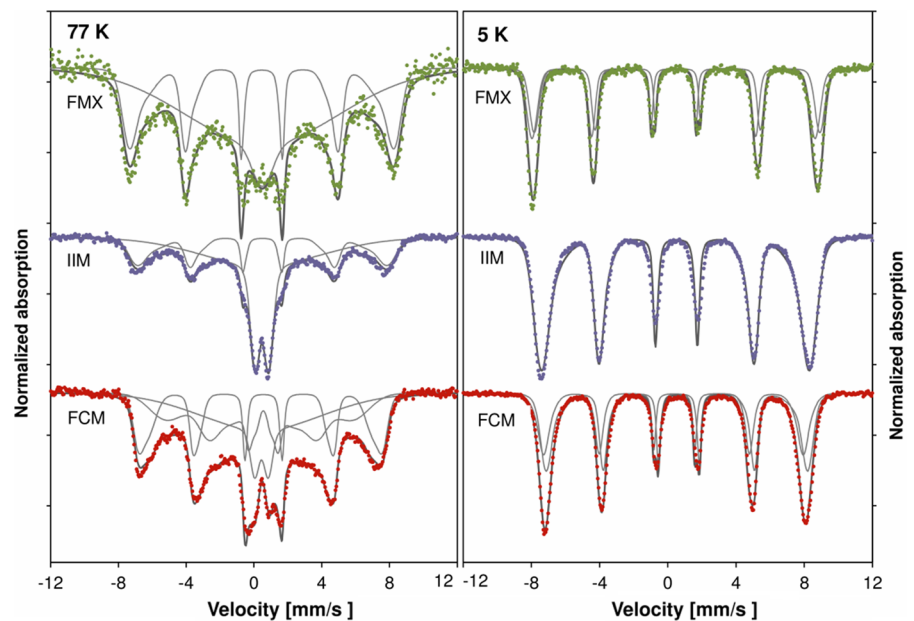


Table 2 Overview of the results from XRD, XANES spectroscopy, and Mössbauer spectroscopy

Sample	XRD		XANES Core mineral	Mössbauer	
	Core mineral	Domain size (nm)		Core mineral	Blocking temperature (K)
FMX	Maghemite ($\gamma\text{-Fe}_2\text{O}_3$)	10	n.d. ^b	Maghemite	73
FCM	Akaganeite ($\beta\text{-FeOOH}$)	4–5	n.d. ^b	Akaganeite	114
IIM	Akaganeite ($\beta\text{-FeOOH}$)	3	Akaganeite	Akaganeite	56
IS	n/a ^a	n/a ^a	Akaganeite	n.d. ^b	n.d. ^b

^a n/a (not applicable): akaganeite most likely but no clear identification of the core mineral by XRD, see text

^b not determined

at 45 K. For higher temperatures an increasing paramagnetic contribution was found. At 245 K, the superparamagnetic doublet was still strongly broadened, showing that the material was not completely superparamagnetic although no distinct sextet features were visible. The coexistence of doublet and sextet features over a large temperature range has been described for nanoparticle suspensions of maghemite (Tronc et al. 2000). The magnetic blocking temperature of FMX was found to be 73 K. The blocking temperature depends mainly on the particle size, crystal structure and interparticle interactions. Based on the assignment as a maghemite suspension, the low blocking temperature of FMX suggests that the iron cores are in the range of 5–10 nm (Morup and Tronc 1994; Tronc et al. 2000).

The Mössbauer spectra of IIM could also be modeled with parameters characteristic for Fe(III), with no indication of the presence of Fe(II). With an average hyperfine field of 47.6 T, IIM showed a significantly weaker hyperfine field at 5 K than FMX (Table S2, Supplementary data). Additionally, some magnetic relaxation, visible as innerline broadening, was present even at 5 K. These spectral features suggest a low crystallinity of the iron cores. The hyperfine field of 47.6 T combined with a center shift of 0.48 mm/s are indicative for an akaganeite structure (Barrero et al. 2006; Bigham et al. 1990). The blocking temperature was 56 K (Table S2, Supplementary data). The spectra between 30 and 60 K showed an increase in paramagnetic contribution, and, at 77 K, 66 ± 1.5 % of the spectral area showed magnetically-

ordered material (Fig. 1). As reported earlier (Jahn et al. 2011), the material is completely paramagnetic at 150 K.

Also the spectra of FCM suggested an akaganeite-like structure without indication of the presence of Fe(II). A second sextet was necessary to model the spectra between 5 and 77 K. The two models used for the spectrum at 5 K had a similar average of the center shift and a slightly weaker magnetic hyperfine field than that of IIM (Fig. 1; Table S2, Supplementary data). The hyperfine field strengths of the sextets were slightly smaller than expected for akaganeite. This could arise from iron on the surface of the mineral cores with a different binding environment compared to bulk material, defects in the akaganeite structure such as chloride vacancies or some additional lepidocrocite in the sample (Bigham et al. 1990; Murad and Cashion 2004). Despite the visible magnetic relaxation at 5 K, which suggests a low crystallinity, the blocking temperature of 114 K was the highest of the three samples. Between 30 and 120 K, both magnetically-ordered material and superparamagnetic

material were present in the sample, while at 245 K the sample was completely paramagnetic, lacking the broadening observed for FMX (data not shown).

X-ray diffraction (XRD)

XRD diffractograms of FMX, recorded for the mannitol-free sample, allowed the identification of the FMX core as a maghemite ($\gamma\text{-Fe}_2\text{O}_3$ space group #96 $P4_32_12$) without any signals of magnetite (Fig. 2a). Models of akaganeite and magnetite worsened the agreement between model and raw data. The best GOF found with maghemite was 6.8, which still represents a lower quality fit. The lattice constants (Table S3, Supplementary data) were in good agreement with reference data for maghemite (Pecharrroman et al. 1995), and the domain sizes were determined to lie around 10 nm, which is in agreement with the Mössbauer data (5–10 nm) and close to the earlier reported core diameter of 6.4 nm (Jahn et al. 2011).

The diffractogram of IS appeared feature-poor with broad peaks, which resulted in an arguable fit with the

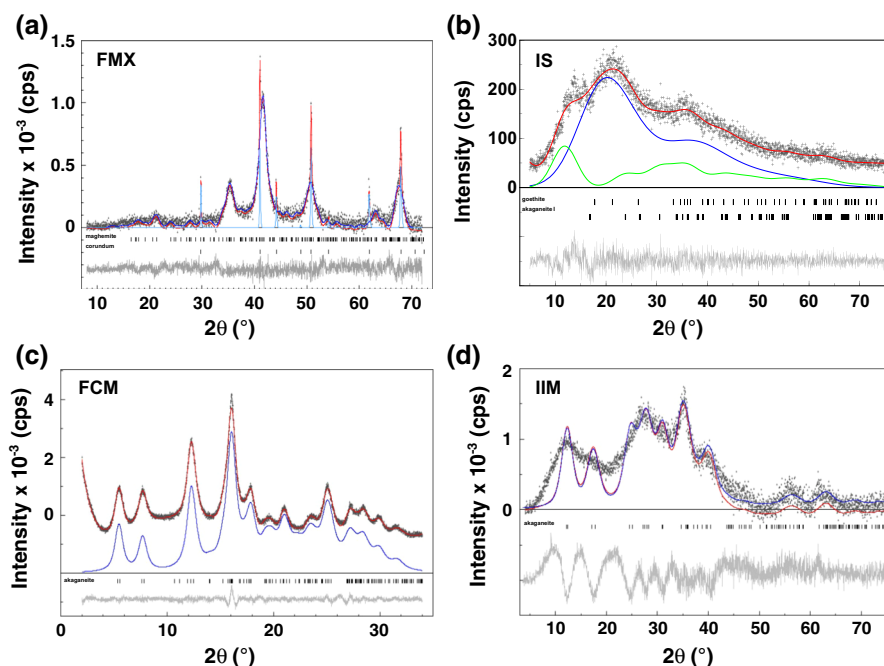


Fig. 2 X-ray diffractograms of FMX (a), IS (b), FCM (c), and IIM (d). The diffractograms show the raw data (grey dots), fitted model (red), sub-patterns of the model phases (blue and green), and in the FMX spectrum (a) also the internal standard corundum (light blue). The model phases are maghemite for

FMX (a), goethite (blue) and akaganeite (green) for IS (b), and akaganeite for FCM and IIM (c, d). Below the diffractograms, the difference curves are shown (grey) and the peak positions of the indicated phases are marked by vertical lines. (Color figure online)

different possible crystallite structures. A mixture of goethite (α -FeOOH, space group #62 Pbnm) and akaganeite (β -FeOOH, space group #12 I2/m) could be postulated (calculated GOF value 1.2) (Fig. 2b). Previously published XRD analyses were interpreted in a variety of different ways: the core structure of IS was assigned as a ferrihydrite (Funk et al. 2001), a ferrihydrite with possibly other structures mixed in such as akaganeite (Jahn et al. 2011), as a lepidocrocite or ferrihydrite (Fütterer et al. 2013), or as akaganeite (Kudasheva et al. 2004). The inconsistency of these results may partly arise from different experimental details such as the drying conditions. Moreover, a very small crystallite size or a low crystallinity in the IS core makes XRD, a technique suitable for the characterization of long-range order, not an ideal method for the investigation of IS. In fact, earlier XRD results suggest a core diameter of between about 1 and 3 nm (Funk et al. 2001; Jahn et al. 2011; Kudasheva et al. 2004).

The mineral core of FCM could clearly be identified as akaganeite (β -FeOOH, space group #12 I2/m) (Fig. 2c; Table 2). The lattice constants (Table S3, Supplementary data) were in good agreement with literature data (Post and Buchwald 1991). The GOF reached 1.4, and the domain size for the akaganeite lay around 4–5 nm, which is in agreement with the value of 4.3 nm reported earlier (Jahn et al. 2011).

The mineral core of IIM could most likely be attributed to an akaganeite-like phase (β -FeOOH, space group #12 I2/m) (Fig. 2d; Table 2). Though accompanied by a large standard deviation, the calculated lattice constants (Table S3, Supplementary data) were in good agreement with reference data for akaganeite (Post and Buchwald 1991). The domain sizes derived were around 3 nm. These results agree well with the previously published description of the IIM core as being similar to akaganeite with a core diameter derived by XRD of 4.2 nm (Jahn et al. 2011). As described for IS, also IIM showed the limitation of XRD for poorly crystalline and/or very small particles. The agreement between model and raw data was poor for all structures tested, which were goethite, lepidocrocite, maghemite and magnetite. The best GOF was obtained by an akaganeite structure with a value of 16.6. The high GOF value and the large variation in the difference curve reflect a low conformity between the applied model and the data, which was observed previously (Jahn et al. 2011).

X-ray absorption near edge structure (XANES) spectroscopy

The relatively broad peaks in the XRD diffractograms and the high GOF values of the described substances show the limitation of XRD for poorly crystalline or very small particles, especially for IS and IIM. Fe K-edge XANES spectroscopy was chosen to better characterize IS and IIM, because it gives information about the short range order of an absorbing element, here Fe, and hence can be applied also for low- or non-crystalline materials. Furthermore, because Fe K-edge XANES measurements were done with liquid samples, artifacts from the drying process, which may play a role especially for the XRD of IS, can be excluded.

The XANES spectra with details of their pre-edge, main-peak and post-edge energy ranges are shown in Fig. 3a–d. It is evident that the curves of the two liquid samples of IIM and IS are deviating significantly from those of goethite, lepidocrocite and ferrihydrites. A good match is observed between the sample spectra and that of akaganeite. Linear combination fits (LCF) confirm that the sample spectra can be described with a major fraction of akaganeite (see Supplementary data, Sect. 2, Figs. S1 and S2, and Table S4). In fact, the best fits are achieved with some ferrihydrite fraction (about 27 % for IS and 17 % for IIM), but do not result in better matches for certain XANES features like the top of the main peak and the pronounced shoulder at the high energy flank of the main peak (Figs. S1a, b, S2a, b, Supplementary data). Hence, this result indicates that the short-range order structures of the iron-containing phase in IS and IIM are similar to akaganeite.

Iron(II) content

Cerimetric titration yielded Fe(II) concentrations relative to the total Fe content of 0.6 % for IIM, 0.8 % for FCM, and 1.0–1.3 % for FMX. These results are consistent with the fact that no Fe(II) was detected in the Mössbauer spectra (detection limit of 1.5–2.5 %) and in the Fe K-edge XANES spectra (detection limit >10 %), and it also agrees with the identification of the FMX, IIM, and FCM core minerals as maghemite (FMX) and akaganeites (IIM, FCM), respectively.

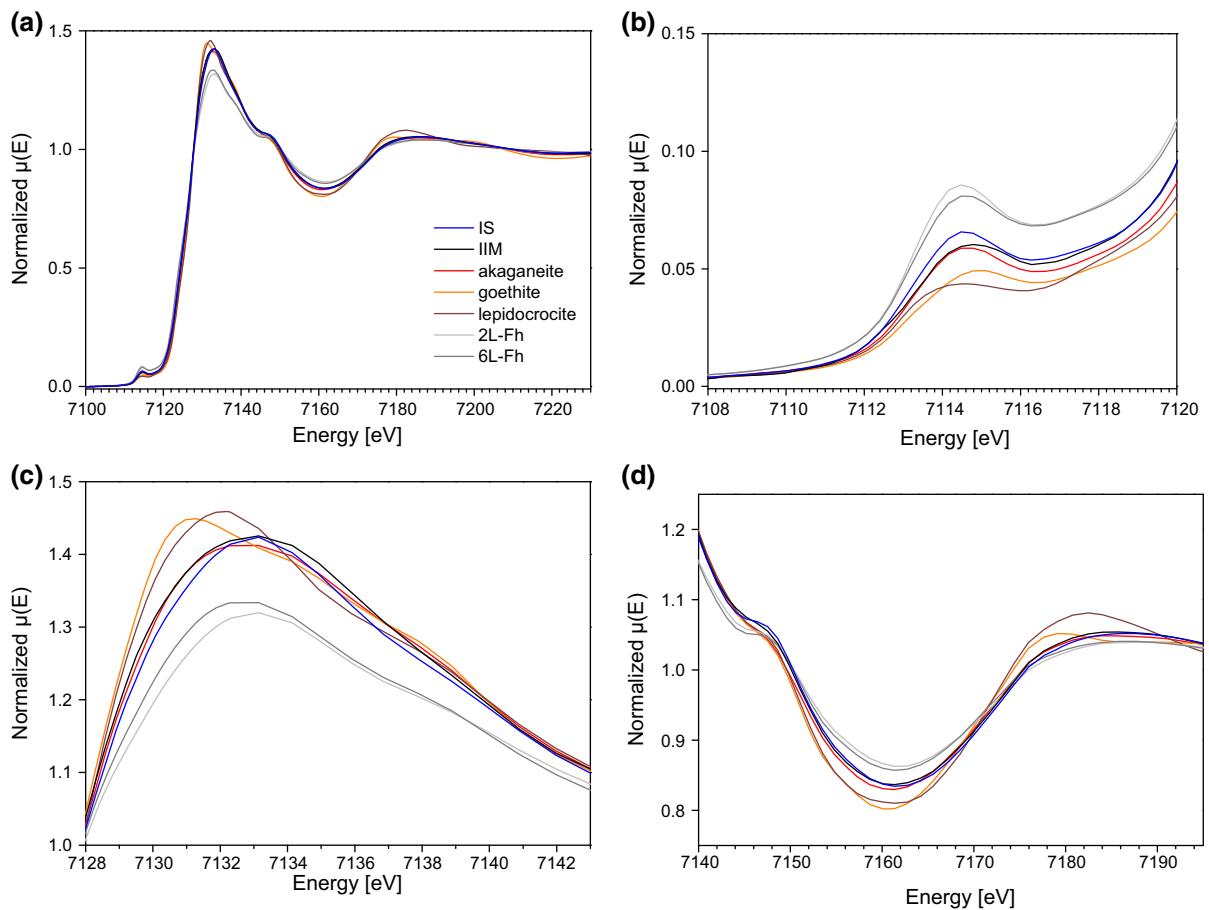


Fig. 3 Fe *K*-edge X-ray absorption near edge structure (XANES) spectra of IS and IIM compared to reference spectra of akaganeite, goethite, lepidocrocite, 2L- and 6L-ferrhydrite (2L-Fh, 6L-Fh): overview of the entire XANES energy range

(a), details from the pre-edge range (b), from the main peak (c), and from the post-edge and beginning EXAFS range (d). The legend in a applies also to (b–d). (Color figure online)

Discussion of the iron core structures

The cores of a number of polynuclear Fe(III)-oxyhydroxide carbohydrate nanoparticles, i.e. iron dextran, iron dextrin, and iron polymaltose have been reported to have akaganeite structures (β -FeOOH) (Funk et al. 2001). Among the new generation IV iron preparations, a nonstoichiometric magnetite structure (Coyne 2009) and an XRD pattern close to that of magnetite and maghemite (Jahn et al. 2011), later reassigned as pure magnetite (Fütterer et al. 2013), have been reported for FMX, whereas an akaganeite structure has been described for FCM and IIM (Jahn et al. 2011). Yet, in the same work (Jahn et al. 2011), the IIM structure has also been described as a “matrix structure” based on ^{13}C NMR data. There seems to

be some confusion in the literature about what exactly is meant with a “matrix structure” (Fütterer et al. 2013; Jahn et al. 2011). A very detailed model with the iron atoms chelated between the carbohydrate chains of the ligand has been presented earlier (Fig. 11 in Jahn et al. 2011), whereas it was recently mentioned that the iron hydroxide is rather stable and this feature has been assigned to the matrix structure (Fütterer et al. 2013). An in-depth NMR study on the carbohydrate–Fe(III) bonding situation in different IV iron preparations, however, disproved the chelation of iron and the matrix structure for IIM, which was stated to derive from an incorrect interpretation of the NMR spectra (Kästele et al. 2014).

The data reported in this work support akaganeite as the core structure of IIM and FCM as well as for IS.

IIM showed a smaller crystallite size than FCM by XRD, which agrees with the wide diffraction lines in the XRD of IIM and the low blocking temperature found by Mössbauer spectroscopy. Earlier XRD data suggested approximately the same crystallite sizes for IIM and FCM of 4.2 and 4.3 nm, respectively (Jahn et al. 2011), which is very close to the values of 3 and 4–5 nm reported here. The Mössbauer spectra of IIM and FCM show comparable hyperfine field parameters at 5 K which are most similar to the parameters of akaganeite. Both materials show some magnetic relaxation at 5 K which suggests a low crystallinity of the iron core. The differences in the magnetic blocking temperatures of IIM and FCM may be explained by a larger size of the iron core or by inter-particle magnetic interaction in FCM at low temperatures, a rationale that has also been given for nano-magnetite suspensions (Morup and Tronc 1994; Tucek et al. 2006). By XRD, the lattice constants of IIM and FCM were also found to be very similar to each other and in good agreement with akaganeite, although the GOF of IIM was rather poor, probably due to its small particle size. Fe K-edge XANES spectra of IIM further confirmed the akaganeite structure of the IIM core. It can thus be concluded that IIM and FCM have akaganeite core structures, but the domain size of IIM is somewhat smaller than that of FCM (Table 2).

For FMX, Mössbauer and XRD data as well as the very low Fe(II) content indicate a maghemite core structure, which is in contrast to previous descriptions of the material as a magnetite (AMAG Pharmaceuticals Inc., Waltham, MA, USA 2009; Coyne 2009) or, also based on XRD investigations, as a structure close to that of magnetite and maghemite (Jahn et al. 2011). In a follow-up paper, Langguth and coworkers (Fütterer et al. 2013) reassigned the structure as pure magnetite based on selected area electron diffraction (SAED) data, by stating that the two structures can be differentiated based on missing rings and respective d -values in the SAED pattern. However, with the presented d -values from the SAED data one can calculate a lattice parameter of 0.844 ± 0.011 nm (space group #227), which does not correspond to magnetite or maghemite. This result is not unexpected, as electron diffraction in transmission electron microscopy (TEM) is not accurate enough to distinguish the minor differences between cubic maghemite (fully or nearly fully oxidized magnetite) and stoichiometric magnetite. In conclusion, a clear differentiation

between magnetite and maghemite can only be done by more appropriate methods, e.g. by Mössbauer spectroscopy. The very low amount of Fe(II) found by cerimetric titration (1.0–1.3 %) as well as the absence of Fe(II) by Mössbauer spectroscopy (detection limit of 1.5–2.5 %) support our assignment of the FMX core structure as maghemite. Finally, the red-brown color of the FMX-solution confirms the assignment as maghemite [pure Fe(III)], as the mixed-valent magnetite would be expected to be black (Cornell and Schwertmann 2003).

The domain size of FMX was approximately 10 and 5–10 nm, derived by XRD and Mössbauer spectroscopy, respectively, and, thus, was found to be larger than that of IIM (about 3 nm) or FCM (4–5 nm) (Table 2) and similar to the 6.4 nm reported earlier (Jahn et al. 2011).

Characterization of the carbohydrate components of IIM and FMX by NMR and GFC

The structures of the carbohydrates isolated from FMX and IIM were identified by 1D and 2D ^1H and ^{13}C NMR investigations. Dextran 1000, Dextran 3–4000, reduced Dextran 3–4000, and reduced and carboxymethylated Dextran 1000 were used as reference materials. In addition to the characterization by NMR spectroscopy, the molecular weight distributions of the isolated carbohydrate components of IIM and FMX were investigated by GFC.

The carbohydrate component of IIM (isomaltoside 1000) could be identified as a linear, low molecular weight, reduced Dextran 1000 (Andreasen and Christensen 2001; Pharmacosmos A/S, Holbaek, Denmark 2009). The NMR spectra of isomaltoside 1000 match the spectra of Dextran 1000 very closely and provide proof for the α -(1 → 6)-linked glucan backbone of dextrans (Fig. 4), but the signals from the reducing glycosides (species C α and C β) are almost completely absent (Fig. 5, Fig. S3, Supplementary data). The resonances of an additional CH₂–OH group could be assigned to a reduced C-1 end unit (species Cred and Cred'), which shows that close to 100 % of the C-1 ends were reduced (Figs. 4, 5). This indicates that no major hydrolysis occurred during the isolation of the carbohydrate. No signs of branched units (1,3-br. or 1,3-br.') were detected in isomaltoside 1000 or in Dextran 1000. The NMR data show that isomaltoside 1000 consists in average of five glycan units with a M_n

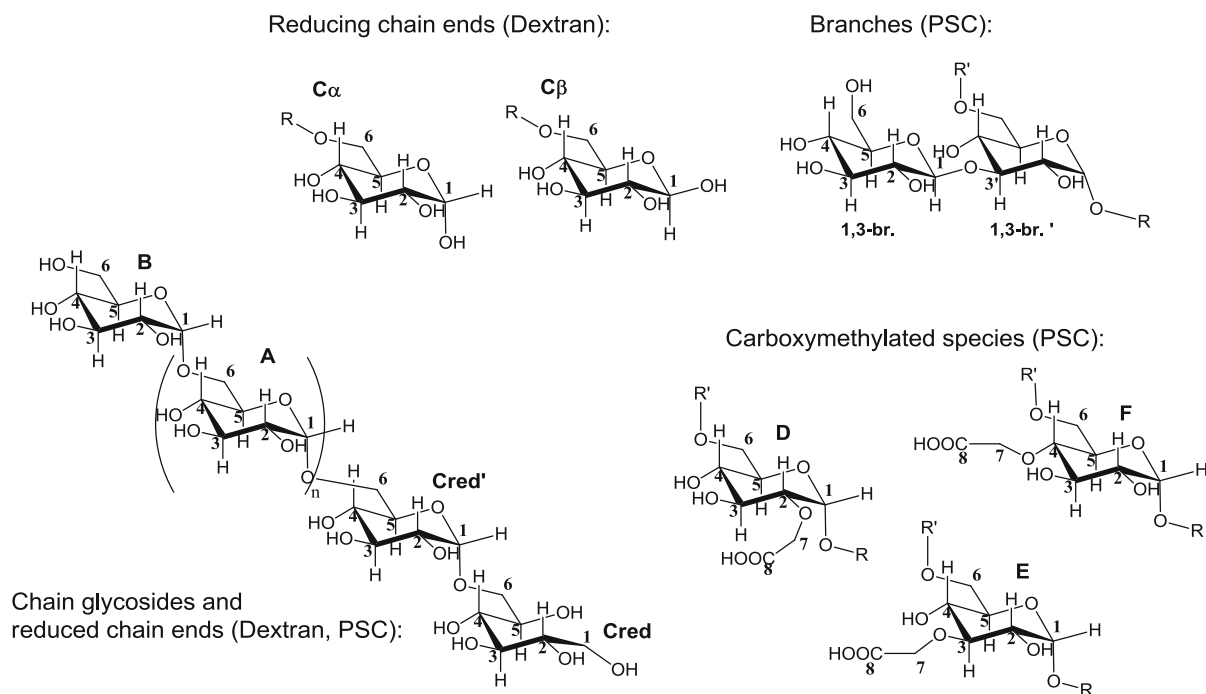


Fig. 4 Different chemical species identified in the carbohydrate components of FMX and IIM and in the dextran reference materials. *R* glycoside polymer

of about 800 Da, which is slightly lower than the chain length of Dextran 1000 from Sigma Aldrich with about 6–7 units and a M_n of about 1100 (Table S5, Supplementary data). For isomaltoside 1000, GFC yielded 1020 and 790 Da for M_w and M_n , respectively (data not shown). The molecular weight distribution parameters obtained for isomaltoside 1000 by GFC are in good agreement with the M_n values derived from NMR measurements and with published information (Andreasen and Christensen 2001; Pharmacosmos A/S, Holbaek, Denmark 2009).

The carbohydrate component of FMX (PSC) was identified as a dextran with a low degree of branching, partly carboxymethylated at positions C-2, C-3, or C-4 in the glucan backbone and with a reduced, non-carboxymethylated C-1 chain end unit. The resonances from species A in the glycoside chain and B at the non-reducing chain end are readily observed, indicating the α -(1 \rightarrow 6)-linked glucan backbone, and a weak resonance at 5.33 ppm provides evidence for a low degree of branching of 1–2 % (species 1,3-br) (Fig. 5, Fig. S3, Supplementary data). In agreement with the description of the FMX carbohydrate by the manufacturer as a polyglucose sorbitol carboxymethylether (European Medicines Agency 2012; Groman et al.

2003) the C-2, C-3 and C-4 carboxymethylated species in the glycoside main chain could be identified by NMR (species D, E, and F). No evidence of carboxymethylation at the primary alcohol group of the C-6 chain end or at the reduced C-1 chain end was found. At the C-1 chain end, all ^1H and ^{13}C NMR resonances characteristic for species Cred (Fig. 4) were detected, implying that the C-1 chain end was reduced but not carboxymethylated (Fig. 5, Fig. S3, Supplementary data). The identity of the carboxymethylated species D, E, F, and of species B and Cred at the glycoside chain ends were unambiguously identified by the NMR analysis of the reduced and carboxymethylated Dextran 1.

A quantitative evaluation of the NMR data suggested that PSC is composed of 20–22 units with a M_n of approximately 3400–3800 Da. The degree of carboxymethylation of the FMX carbohydrate was determined to lie around 0.18–0.23, which corresponds to one carboxymethylated unit for every 4–5 glycan units (Table S5, Supplementary data). The determination of the molecular weight distribution by GFC yielded a M_w of 14.2 kDa, a M_n of 8.2 kDa, and a polydispersity (P) of 1.73 (data not shown). The observed discrepancy between the M_n value obtained by GFC and that obtained by NMR is probably at least

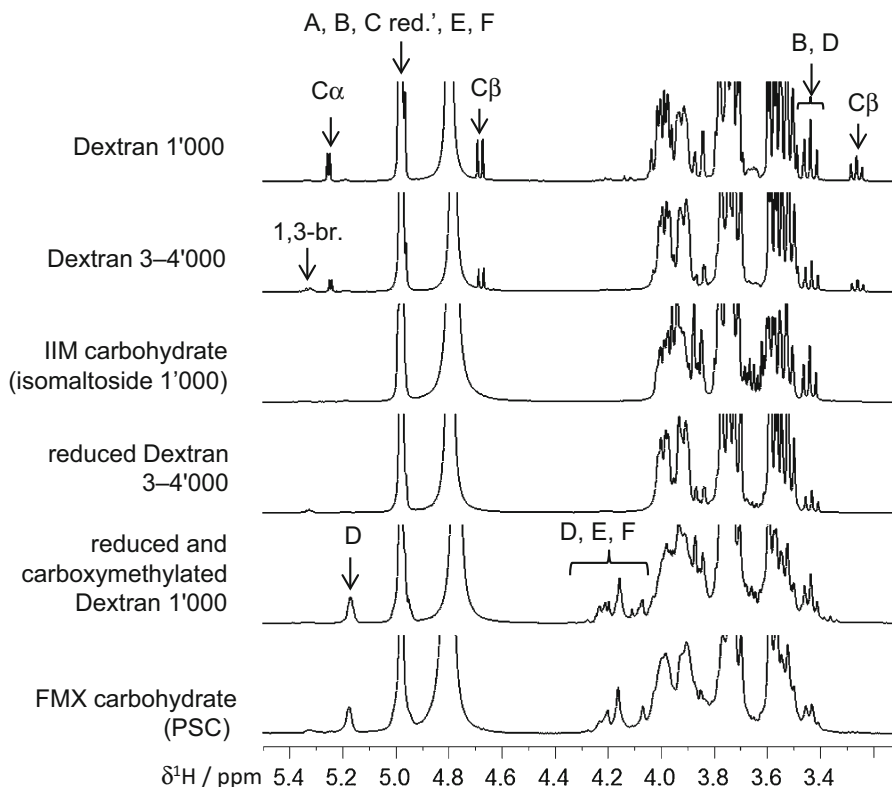


Fig. 5 Regions of interest of 1D ^1H NMR spectra of the carbohydrate components of IIM and FMX and of the different reference dextrans with assignments to chemical species shown in Fig. 4. Characteristic spectral regions and number of protons contributing to the signal intensities: 5.33 ppm (1,3-br., 1 H),

5.24 ppm ($\text{C}\alpha$, 1 H), 5.18 ppm (D, 1 H), 4.98 ppm (A, B, Cred', E and F, 1 H each), 4.67 ppm ($\text{C}\beta$, 1 H), 4.00–4.25 ppm (D, E and F, 2 H each), 3.45 ppm (B and D, 1 H each), 3.26 ppm ($\text{C}\beta$ 1 H)

partly due to the higher excluded volume (i.e. lower apparent density) of a carboxymethylated dextran relative to that of a native dextran.

It is conceivable that the conditions applied for the isolation of the carbohydrates of FMX and IIM, a heat treatment at 132 °C and pH 5.4, may induce the degradation of polysaccharides. Yet, the observation that no NMR-resonances belonging to the reducing C-1 chain end units were detected in the spectra of the FMX or IIM carbohydrates indicates that degradation did not occur to a significant extent.

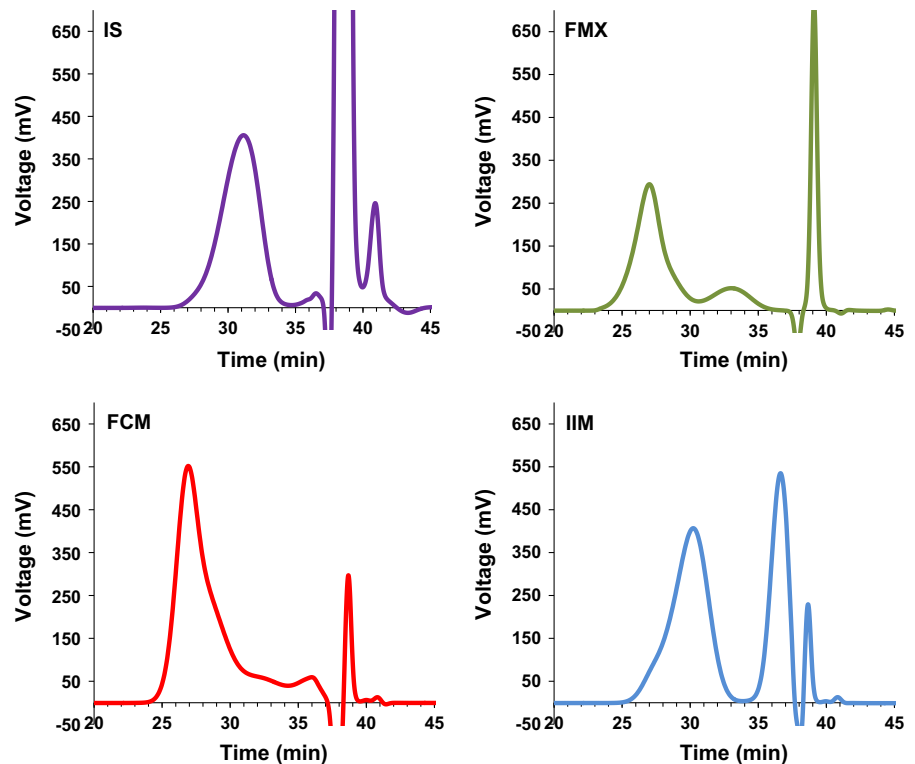
Characterization of the iron-carbohydrate nanoparticles

Molecular weight distribution by GFC

GFC yielded the highest M_w values for FMX (172–188 kDa, five lots analyzed), followed by FCM

(145–155 kDa, two lots), IIM (63–69 kDa, three lots), and IS (42–44 kDa, two lots). In the chromatograms of all preparations, the first eluted fraction with the highest molecular weight average corresponds to the iron-carbohydrate nanoparticles (Fig. 6). For FCM, IIM, and FMX, further fractions, which eluted after the first fraction and before the negative solvent peak, can be assigned to weakly-bound or dissociated carbohydrate. The position of these peaks (or shoulder, in the case of FCM) is in good agreement with the molecular weight of the respective stabilizing carbohydrates. Carboxymaltose (in FCM) and PSC (in FMX) have a higher molecular weight and therefore elute earlier than isomaltoside 1000 in IIM. Since the FMX solution contains additional PSC as an excipient (European Medicines Agency 2012), the observed peak also includes this material. In the case of IIM, the carbohydrate peak probably also contains the citrate which is mentioned as an additional stabilizing

Fig. 6 Gel filtration chromatography of IS (Venofer[®] lot 091201), FCM (Ferinject[®] lot 169001), FMX (Feraheme[®] lot A56996A), and IIM (MonoFer[®] lot 042838-3). (Color figure online)



compound by the manufacturer (Medice Pharma GmbH&Co. KG, Iserlohn, Germany 2011) and which elutes together with isomaltoside 1000. The material eluted after the solvent peak stems from components with a significantly smaller molecular weight. For IS, two peaks are found after the solvent peak, the larger one corresponding to sucrose and chloride, and the smaller peak probably to a mixture of hydroxide and carbonate. In the FCM and the IIM chromatograms, the last peak arises from chloride which is present in the two solutions in comparable amounts. Finally, the last peak of the FMX chromatogram has been assigned to mannitol, which is a further excipient in the FMX solution [44 mg/mL, (AMAG Pharmaceuticals Inc., Waltham, MA, USA 2009)].

The relative order of the M_w values is in agreement with previously published data (Balakrishnan et al. 2009; Jahn et al. 2011), but the shapes of the chromatograms and the absolute values are different. For instance, a large discrepancy was noticed between the M_w values reported for FMX, i.e. 731 kDa (Balakrishnan et al. 2009), 275.7 kDa (Jahn et al. 2011), and 172–188 kDa (this work). This variation can be explained by the use of different standards, i.e. protein

(Balakrishnan et al. 2009) and dextran (Jahn et al. 2011) standards instead of the pullulan standards used in the USP method (U.S. Food and Drug Administration 2012b) and in this work. Since the apparent density of the investigated compounds does not correspond to any of these standards, none of the reported values of the molecular weight represents an absolute measure, but they allow for a relative comparison between the samples' hydrodynamic volume. The different results for M_w are therefore not necessarily contradictory. Nevertheless, it is important to note that M_w values of different compounds can only be compared when measured relative to the same standard, a guidance that is not always followed (Munoz and Martin-Montanez 2012; Pai and Garba 2012; Rosner and Auerbach 2011).

Also the shapes of the reported elution profiles for the various preparations differ among publications. In an earlier report (Jahn et al. 2011), the peak of the highest molecular weight component for FMX was observed close to the elution volume, as indicated by the authors. Thus, this peak as well as the shoulder observed at the same position for FCM probably are artifacts resulting from non-separation of higher molecular weight components. Furthermore, the lower

molecular weight components detected in this work in the IS and IIM chromatograms (Fig. 6) have not been detected in the earlier report (Jahn et al. 2011). The exact reason for this discrepancy is not clear, as the full experimental details have not been reported by Jahn et al. but it can most likely be explained by different experimental details, such as the choice of the column, detector and/or solvent.

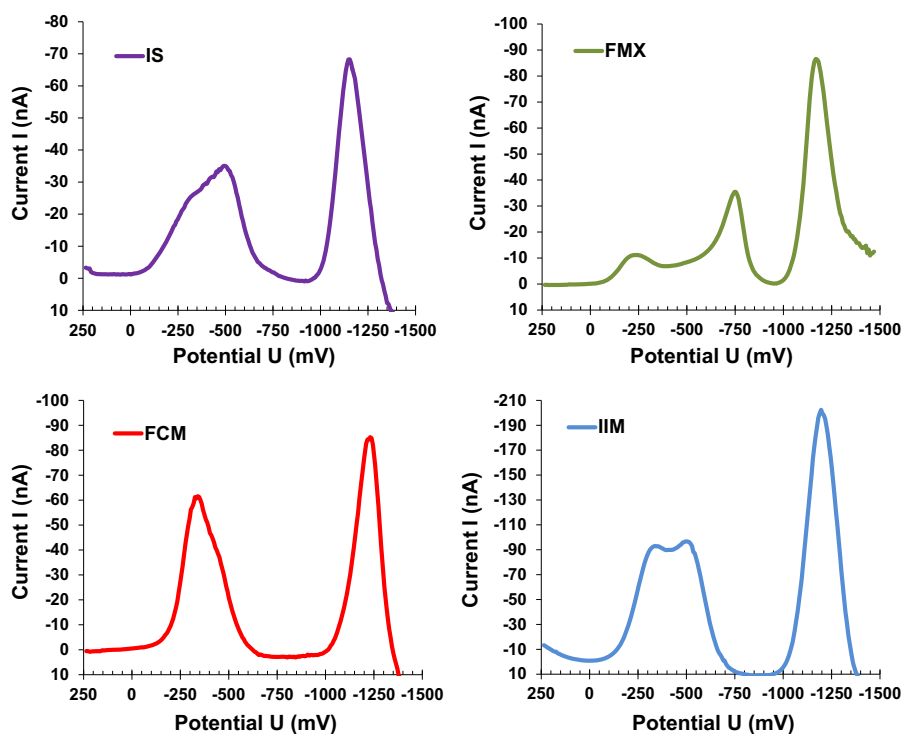
Polarographic analysis

Polarographic analysis showed for all compounds the two expected transitions, i.e. Fe(III)/Fe(II) and Fe(II)/Fe(0) (Merli et al. 2012; U.S. Food and Drug Administration 2012b), but the shape and the maxima of the first reduction peaks were characteristic for each preparation (Fig. 7; Table S6, Supplementary data). In the range between -100 and -700 mV, FCM showed the narrowest and the most uniform peak with only a slight shoulder. For IS, the Fe(III)/Fe(II) peak in this range was much broader, whereas IIM showed a double peak with two nearly equally intense responses. In the intermediate potential range between about -700 and -1000 mV there were essentially no transitions for IS, FCM, and

IIM. The values of the reduction potential for IS and FCM differ to some extent from those reported earlier (Crichton et al. 2008), which were recorded in a TRIS-buffered solution at pH 7.4 for FCM and an acetate-buffered solution at pH 6 for IS (Vifor (International) Ltd., internal reports).

In contrast, FMX showed a completely different pattern with two well separated reduction bands in the range between -50 and -1000 mV, with the more positive peak (max. around -250 mV) being less pronounced than the more negative peak (max. around -740 mV). A control measurement demonstrated that mannitol, present in rather large amounts as an excipient in FMX, does not show any reduction wave in the studied range (data not shown). The polarograms of all compounds showed very similarly positioned peaks for the Fe(II)/Fe(0) transitions in the range -1000 to -1400 mV. It has recently been claimed that the second peak in the polarogram of IS cannot be attributed to the Fe(II)/Fe(0) transition, but arises from adsorption processes (Mahmoudi and Kissner 2014). However, these polarographic analyses (Mahmoudi and Kissner 2014) were carried out with a different technique, a different electrode and, importantly, at a different pH

Fig. 7 Polarograms of FMX (Feraheme[®] lot 1061002), IIM (MonoFer[®] lot 042838-3), IS (Venofer[®] lot 091201), and FCM (Ferinject[®] lot 169001). Potentials are given versus SHE; the reduction potentials are given in Table S6, Supplementary data. (Color figure online)



than those described in our study as well as in the current USP (Merli et al. 2012). Thus, the relevance of these results for the present discussion is questionable.

The two distinct reduction bands for Fe(III)/Fe(II) in the FMX polarogram suggest at least two types of Fe(III) with a chemical environment with substantially different electronic properties. Possibly, the Fe(III) of the inner core of the polynuclear Fe(III)-oxide (maghemite) is more stable towards reduction, i.e. has a more negative reduction potential, than that on the surface. This property could be explained by the strong coordination of Fe(III) with oxide ions (O^{2-}) in the center of the core, as opposed to the coordination of Fe(III) with hydroxide and/or water at the surface of the polynuclear iron core. FCM, IIM (Jahn et al. 2011, this work), and IS have polynuclear iron(III)-oxyhydroxide cores with an akaganeite structure. The double peak present in the polarograms of IIM and IS but not in that of FCM seems therefore not likely to be caused by structural differences in the inner akaganeite core of the particles. The differences in the polarograms may arise from different types of iron-carbohydrate interactions, as well as from the different particle shapes (Jahn et al. 2011), which may cause different surface properties. Overall, the polarograms illustrate that the stability and the electronic environment in the Fe(III) cores is different and distinct for each preparation. Thus, the polarogram can be regarded as a fingerprint of the iron cores' structure and carbohydrate interactions, as well as the thermodynamic stability of the cores (Toblli et al. 2012).

Reductive degradation kinetics

The kinetic stability of IIM, FCM, and FMX was evaluated under acidic conditions in presence of ascorbic acid (Fig. 8). The values of $k(\theta)$ at 10, 50, and 80 % of degradation ($\theta = 0.1, 0.5, \text{ and } 0.8$) are given in Table S7 (Supplementary data). The kinetics observed for IIM was comparable and in the same range as the values previously reported for different iron dextrans (Geisser et al. 1992). In contrast, FMX showed faster reductive degradation kinetics. All three compounds (FMX, IIM, FCM) show progressive, i.e. accelerating, kinetics with increasing rate constants (Fig. 8; Table S7, Supplementary data) in agreement with the behavior expected for approximately monodisperse compounds (Erni et al. 1984; Geisser et al. 1992).

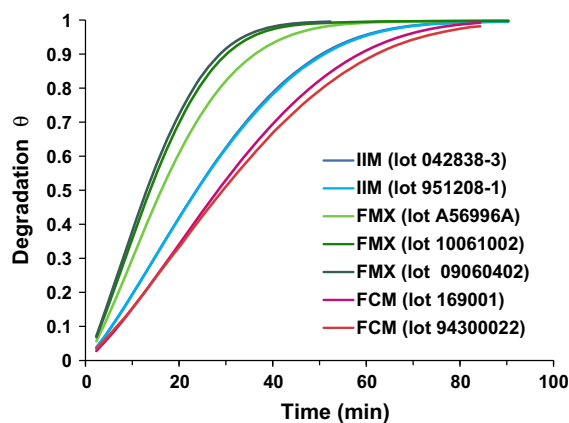


Fig. 8 Reductive degradation kinetics shown as the extent of decomposition (θ) of IIM, FCM, and FMX as a function of time. The two curves for IIM are nearly congruent. Calculated according to Erni et al. (1984). (Color figure online)

IV iron compounds with slow degradation kinetics [$k(\theta) = (15\text{--}50) \times 10^3 \text{ min}^{-1}$, $\theta = 0.5$] have been classified as robust (Geisser et al. 1992; Geisser and Burckhardt 2011). This property was foreseen for FCM and IIM, based on previously reported kinetics of acid degradation (Jahn et al. 2011). However, the faster degradation of FMX seems to be in contrast to the data on acid decomposition kinetics, which was slower for FMX than for IIM and FCM (Jahn et al. 2011). Evidently, although FMX is very resistant against acid hydrolysis, it is more susceptible to reductive degradation than IIM and FCM.

For the first generation of IV iron preparations, a correlation was observed between the reductive degradation kinetics and the M_w value (Geisser et al. 1992). This observation led to the classification of these compounds into four types according to their kinetic and thermodynamic stability and M_w (Geisser et al. 1992). However, the correlation between M_w and degradation kinetics does not apply to FMX, which should be classified as strong and robust (Type I) according to its M_w of about 180 kDa but showed the relatively faster reductive degradation kinetics of a semi-robust and moderately strong (Type II) compound. On the other hand, the M_w of IIM (63–69 kDa) is typical for Type II compounds, whereas its reduction kinetics is that of a Type I compound. Therefore, this classification as well as the correlation between the M_w and the iron release kinetics (Geisser et al. 1992) cannot be strictly applied to the newest generation of IV iron compounds.

Labile or weakly-bound iron

All IV iron preparations contain a certain percentage of iron which is not strongly bound to the core. Upon IV administration, this labile (or weakly-bound) iron is likely to be immediately transferred to transferrin and, if present in excess of transferrin's iron binding capacity, it may lead to the formation of non-transferrin-bound iron (NTBI) (Koskenkorva-Frank et al. 2013).

As shown in Fig. 9, the content of labile iron in the various IV iron preparations can be visualized in a qualitative way by mixing the iron solutions with white tea. Polyphenols in tea react with labile Fe(II) and Fe(III) species to form iron complexes which appear as a suspension of red-brown to black particles. Reaction of different IV iron preparations with the tea extract at equal iron concentrations and without adjustment of the pH (final range: pH 5.0–6.9) allowed for a classification of the preparations according to their content of labile iron. Due to the strong characteristic color of the various IV iron preparations, all of the mixtures have a more intense brown coloration than the blank tea sample. Very little visible additional discoloration was observed for FCM, FMX, and IIM, whereas a clearly visible discoloration and turbidity could be detected with IS and SFG (Fig. 9). Thus, this simple experiment shows, although only qualitatively, the presence of higher amounts of labile iron in SFG and IS than in IIM, FMX, and FCM, a result that is in agreement with quantitative measurements of labile iron (Fig. 9 and references cited therein).

Labile iron can be mobilized from the surface of a polynuclear iron core by complex-forming agents and has been quantified with a variety of chelators such as EDTA (Jahn et al. 2007), ferrozine (Jahn et al. 2011; Stefansson et al. 2011) or transferrin (Van Wyck et al.

2004). Notably, depending on their affinity for iron, these chelators may also partly mobilize more strongly bound iron from the core and lead to artificially high values for labile iron. Therefore, the various methods used to measure labile iron often yield different absolute amounts for the same IV iron preparation (Table 3 and references cited therein). Nevertheless, the reported amounts of labile iron are mostly in the same order of magnitude and relative differences obtained with the various methods are comparable.

In some studies, when comparing the properties of different IV iron preparations, a distinction was made between “free” and labile iron (Jahn et al. 2011). Free iron was used as a synonym for dialyzable iron present in diluted iron preparations (Balakrishnan et al. 2009; Jahn et al. 2011) which was quantified either by ultrafiltration with a molecular weight cut-off of 30 kDa (Balakrishnan et al. 2009) or by dialysis (with a tubing cut-off of 12–14 kDa) (Balakrishnan et al. 2009; Jahn et al. 2011). Clearly, under these experimental conditions, the measurement of free iron includes oligomeric forms with a high molecular weight up to the selected cut-off. In both cases, the relative amount of free iron for the different IV iron preparations was not in agreement with the labile iron results (Table 3). In particular, IS showed significantly lower amounts of free iron than iron dextran (Balakrishnan et al. 2009; Jahn et al. 2011), a result that is difficult to rationalize with the known physico-chemical and clinical data and thus questions its validity. Notably, for all preparations the absolute amounts of free iron were very low, and thus it was concluded that free iron is not likely to induce the formation of NTBI in the blood. Importantly, the amount of free iron is included in the quantification of the labile iron (Balakrishnan et al. 2009; Jahn et al. 2011), which thus is a much more relevant parameter.

Fig. 9 Visualization of labile iron content by mixing iron preparations (0.1 mg Fe/mL) with white tea. Labile or “free” iron reacts with polyphenols in tea to form a suspension of red-brown to black iron complex particles. (Color figure online)

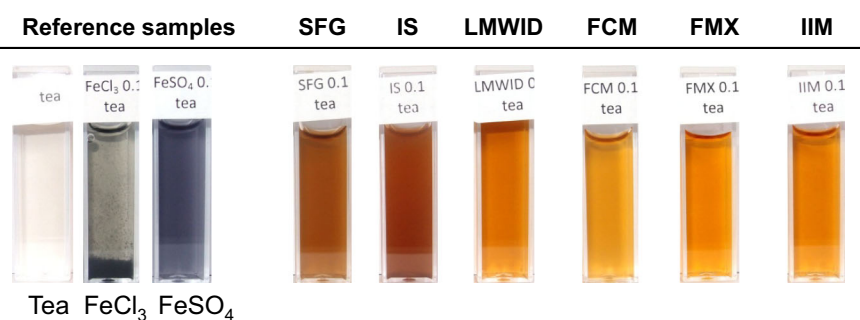


Table 3 Labile or “free” iron content in IV iron preparations assessed by different analytical methods

Quantified parameter/Method	Unit	SFG	IS	LMWID	FCM	FMX	IIM	Ref.
Labile, weakly-bound iron								
EDTA in vitro								
1 min	(%)	2.1	1.1	0.4	n/a	n/a	n/a	Jahn et al. (2007)
19.3 h	(%)	4	4	1	n/a	n/a	n/a	Jahn et al. (2007)
Ferrozine in vitro (human serum)								
	(%)	3.2	3.5	2	0.5	1	1	Jahn et al. (2011)
	(%)	n/a	5.6	1.6	n/a	n/a	n/a	Stefansson et al. (2011)
Ferrozine in vivo (humans)	(μ M)	n/a	27.9	7.4	n/a	n/a	n/a	Stefansson et al. (2011)
Transferrin in vitro	(%)	5.8	4.5	3.4	n/a	n/a	n/a	Van Wyck et al. (2004)
Bleomycin-detectable iron								
Rat serum	(%)	1.4	0.69	0.19	n/a	0.07	n/a	Balakrishnan et al. (2009)
Human serum	(%)	0.96	0.89	0.40	n/a	0.15	n/a	Balakrishnan et al. (2009)
Rat in vivo	(μ M)	1.69	0.92	0.65	n/a	0.33	n/a	Balakrishnan et al. (2009)
Dialyzable/filterable iron								
Ultrafilterable iron (no pH adjustment, MWCO 30 kDa)								
Dialysis (MWCO 12–14 kDa)								
pH 7	(%)	1.338	0.067	0.207	<0.002	<0.002	<0.002	Jahn et al. (2011)
no pH adjustment	(%)	n/a	n/a	0.172	0.262	0.005	0.014	Jahn et al. (2011)
Hemodialyzer (phosphate buffer)	(%)	5	3	<1.0	n/a	<1.0	n/a	Balakrishnan et al. (2009)

FCM, ferric carboxymaltose; FMX, ferumoxytol; IIM, iron isomaltoside 1000; IS, iron sucrose; LMWID, low molecular weight iron dextran; MWCO, molecular weight cut-off; n/a, not available; Ref., reference; SFG, sodium ferric gluconate

“Free” iron is a frequently encountered term in the medical literature which, unfortunately, is used indistinguishably as a synonym for labile (Pai and Garba 2012; Steen et al. 2013; von and Adamson 2012) and dialyzable iron in IV iron preparations (Balakrishnan et al. 2009; Jahn et al. 2011; Van Wyck 2004), as well as for bleomycin-detectable iron (often also called catalytic iron) (Balakrishnan et al. 2009; Zager et al. 2004) and NTBI (Stefansson et al. 2011). From a chemistry point of view, free iron is defined as $[\text{Fe}(\text{H}_2\text{O})_6]^{2+}$ or $[\text{Fe}(\text{H}_2\text{O})_6]^{3+}$, and their deprotonated forms (Balakrishnan et al. 2009; Jahn et al. 2011). Because of the large values of the acid dissociation constant of water coordinated to Fe(III) ($\text{pK}_a = 2.2$) (Lippard and Berg 1994), deprotonated species are generated even at low pH values. These species rapidly dimerize, oligomerize, and lead to precipitation of the formed Fe(III)-hydroxo complexes (Crichton 2009; Lippard and Berg 1994). Noteworthy, at pH 7.0 $[\text{Fe}(\text{H}_2\text{O})_6]^{3+}$ exists in solution only at concentrations $\leq 10^{-18}$ M (Crichton 2009), and the concentration of free iron (in its Fe(III) form) is maximally around

10^{-10} M (Cornell and Schwertmann 2003). Under physiological conditions, significant concentrations of water-soluble Fe(III)-species can only be obtained in the presence of strong chelating ligands (Crichton 2009; Lippard and Berg 1994). The reduced form $[\text{Fe}(\text{H}_2\text{O})_6]^{2+}$ is more soluble but is rapidly (auto)oxidized under physiological conditions (Crichton 2009; Koskenkorva-Frank et al. 2013). Thus, discussions about free iron are meaningless, and the analysis of free iron (as dialyzable iron) in IV iron preparations at a pH 5–11 also quantifies oligomers generated during the long dialysis procedure (up to 24 h) (Balakrishnan et al. 2009; Jahn et al. 2011).

In summary, the different methods, including the qualitative tea-test experiment, show similar trends of labile iron contents with $\text{SFG} \geq \text{IS} > \text{LMWID} \geq \text{FMX} \approx \text{IIM} \approx \text{FCM}$, which roughly mirrors the maximal recommended single doses of the different preparations (Table 1). Thus, if applied at the recommended doses, all IV iron preparations should lead only to a minimal, transient formation of NTBI (Koskenkorva-Frank et al. 2013).

Conclusion

All IV iron preparations are colloidal solutions of compounds made of polynuclear Fe(III)-(oxyhydr)oxide cores stabilized by carbohydrates. Although the active ingredients are rather similar, and the products are used for similar indications, clinically-relevant properties such as their maximum recommended doses and serum terminal half-lives are significantly different. These dissimilarities among iron-based nano-colloidal products are not surprising because the nanoparticles vary in structure and size as well as in the type and strength of bonds between the core and the stabilizing carbohydrates (Geisser et al. 1992; Kästele et al. 2014). The particle core as well as the carbohydrates (except for IS and SFG) are polymers, each with a specific molecular weight distribution and, therefore, the exact characterization of these compounds is accordingly difficult. This problem has recently been recognized by the regulatory authorities, and there is an ongoing discussion regarding the minimal requirements for approval of intended copies of NBCD (Borchard et al. 2012; Crommelin et al. 2014; Schellekens et al. 2014). For the registration of a generic form of an IV iron preparation such as IS and SFG, the FDA requires a number of analyses in addition to those that are given in the monographs (U.S. Food and Drug Administration 2012a, 2013). Techniques used in this work, such as polarography, XRD, and Mössbauer spectroscopy, have been mentioned by the FDA in the context of a better characterization of SFG (Woodcock 2011). The conflicting XRD results for the IS core reported in different studies apart from this work (Funk et al. 2001; Jahn et al. 2011; Kudasheva et al. 2004) further illustrate the difficulty to accurately characterize these materials. We demonstrated that Fe K-edge XANES spectroscopy is helpful to characterize the poorly crystalline samples, a result which highlights the importance of the right choice of the applied methods. Finally, we showed that the molecular weight distribution parameters strongly depend on the standards used for the calibration of the chromatography column and do not represent absolute values. Clearly, more work is needed to elucidate the exact cellular uptake and degradation mechanisms of nano-colloidal IV iron preparations in order to determine which physico-chemical properties are fundamental for their clinical safety and efficacy.

Acknowledgments We thank Werner Agster, Zorica Nikolic, Roland Riederer, and Maja Thum (all Vifor (International) Ltd.) for technical assistance. We are also grateful to Ralf Weigel from ANKA–Synchrotron Radiation Facility, Karlsruhe Institute for Technology (KIT), for constructing the cell for liquid samples used in Fe K-edge XANES spectroscopy. Dr. Peter Geisser, Vifor (International) Ltd., is thanked for valuable discussions.

Conflict of interest S. Neiser, M. Wilhelm, M. Braitsch, F. Funk, E. Philipp, and S. Burckhardt are employees of Vifor (International) Ltd. D. Rentsch investigated the structure of the carbohydrate components by NMR, U. Dippon and A. Kappler examined the core structures by Mössbauer spectroscopy, P. Weidler investigated the core structures by XRD, and J. Götlicher and R. Steininger examined the core structures by Fe K-edge XANES. The measurements for these studies were paid for by Vifor (International) Ltd.

References

- AMAG Pharmaceuticals Inc., Waltham, USA (2009) Feraheme prescribing information. http://www.accessdata.fda.gov/drugsatfda_docs/label/2009/022180lbl.pdf. Accessed 19 July 2013
- Andreasen HB, Christensen L (2001) Iron-dextran compound for the use as component in a therapeutical composition for prophylaxis or treatment of iron-deficiency. Patent US 6291,440
- Auerbach M, Ballard H (2010) Clinical use of intravenous iron: administration, efficacy, and safety. *Hematol Am Soc Hematol Educ Progr* 2010:338–347
- Avni T, Leibovici L, Gafter-Gvili A (2012) Iron supplementation for the treatment of chronic heart failure and iron deficiency: systematic review and meta-analysis. *Eur J Heart Fail* 14:423–429
- Balakrishnan VS, Rao M, Kausz AT, Brenner L, Pereira BJ, Frigo TB, Lewis JM (2009) Physicochemical properties of ferumoxytol, a new intravenous iron preparation. *Eur J Clin Invest* 39:489–496
- Barrero C, Garcia K, Morales A, Kodjikian S, Greneche J (2006) New analysis of the Mössbauer spectra of akaganeite. *J Phys* 18:6827–6840
- Besarab A, Coyne DW (2010) Iron supplementation to treat anemia in patients with chronic kidney disease. *Nat Rev Nephrol* 6:699–710
- Bigham JM, Schwertmann U, Carlson L, Murad E (1990) A poorly crystallized oxyhydroxysulfate of iron formed by bacterial oxidation of Fe(II) in acid-mine waters. *Geochim Cosmochim Acta* 54:2743–2758
- Borchard G, Flühmann B, Mühlebach S (2012) Nanoparticle iron medicinal products: requirements for approval of intended copies of non-biological complex drugs (NBCD) and the importance of clinical comparative studies. *Regul Toxicol Pharmacol* 64:324–328
- Breyman C, Honegger C, Holzgreve W, Surbek D (2010) Diagnosis and treatment of iron-deficiency anaemia during pregnancy and postpartum. *Arch Gynecol Obstet* 282:577–580

- Chertow GM, Mason PD, Vaage-Nilsen O, Ahlmen J (2006) Update on adverse drug events associated with parenteral iron. *Nephrol Dial Transpl* 21:378–382
- Cornell RM, Schwertmann U (2003) The iron oxides; structure, properties, reactions, occurrences, and uses. Wiley-VCH, Weinheim
- Coyne DW (2009) Ferumoxytol for treatment of iron deficiency anemia in patients with chronic kidney disease. *Expert Opin Pharmacother* 10:2563–2568
- Crichton R (2009) Iron metabolism from molecular mechanisms to clinical consequences. Wiley, Chichester
- Crichton RR, Danielson BG, Geisser P (2008) Iron therapy with special emphasis on intravenous administration. UNI-MED, Bremen
- Crommelin DJ, de Vlieger JS, Weinstein V, Mühlebach S, Shah VP, Schellekens H (2014) Different pharmaceutical products need similar terminology. *AAPS J* 16:11–14
- Erni I, Oswald N, Rich HW, Schneider W (1984) Chemical characterization of iron (III)-hydroxide-dextrin complexes. A comparative study of commercial preparations with alleged reproductions used in the examination of bioavailability. *Arzneimittelforschung* 34:1555–1559
- European Medicines Agency (2012) CHMP Assessment Report Rienso; Common name: ferumoxytol; Procedure No.: EMEA/H/C/002215. http://www.ema.europa.eu/docs/en_GB/document_library/EPAR_-_Public_assessment_report/human/002215/WC500129751.pdf. Accessed 26 Mar 2013
- Funk F, Long FG, Hautot D, Büchi R, Christl I, Weidler PG (2001) Physical and chemical characterization of therapeutic iron containing materials: a study of several superparamagnetic drug formulations with the beta-FeOOH or ferrihydrite structure. *Hyperfine Interact* 136:73–95
- Fütterer S, Andrusenko I, Kolb U, Hofmeister W, Langguth P (2013) Structural characterization of iron oxide/hydroxide nanoparticles in nine different parenteral drugs for the treatment of iron deficiency anaemia by electron diffraction (ED) and X-ray powder diffraction (XRPD). *J Pharm Biomed Anal* 86C:151–160
- Gafter-Gvili A, Rozen-Zvi B, Vidal L, Leibovici L, Vansteenkiste J, Gafter U, Shpilberg O (2013) Intravenous iron supplementation for the treatment of chemotherapy-induced anaemia—systematic review and meta-analysis of randomised controlled trials. *Acta Oncol* 52:18–29
- Geisser P, Burckhardt S (2011) The pharmacokinetics and pharmacodynamics of iron preparations. *Pharmaceutics* 3:12–33
- Geisser P, Baer M, Schaub E (1992) Structure/histotoxicity relationship of parenteral iron preparations. *Arzneimittelforschung* 42:1439–1452
- Gomollon F, Gisbert JP (2013) Intravenous iron in inflammatory bowel diseases. *Curr Opin Gastroenterol* 29:201–207
- Goodnough LT, Nemeth E, Ganz T (2010) Detection, evaluation, and management of iron-restricted erythropoiesis. *Blood* 116:4754–4761
- Groman, EV, Paul, KG, Frigo, TB, Bengel, H, Lewis, JM (2003) Heat stable colloidal iron oxides coated with reduced carbohydrates and carbohydrate derivatives. Patent US 6,599,498
- Haththotuwa R, Goonewardene M, Desai S, Senanayake L, Tank J, Fraser IS (2011) Management of abnormal uterine bleeding in low- and high-resource settings: consideration of cultural issues. *Semin Reprod Med* 29:446–458
- Jahn MR, Mrestani Y, Langguth P, Neubert RH (2007) CE characterization of potential toxic labile iron in colloidal parenteral iron formulations using off-capillary and on-capillary complexation with EDTA. *Electrophoresis* 28:2424–2429
- Jahn MR, Andreassen HB, Fütterer S, Nawroth T, Schünemann V, Kolb U, Hofmeister W, Munoz M, Bock K, Meldal M, Langguth P (2011) A comparative study of the physico-chemical properties of iron isomaltoside 1000 (Monofer), a new intravenous iron preparation and its clinical implications. *Eur J Pharm Biopharm* 78:480–491
- Jander G, Jahr KF, Schulze G, Simon J (2003) Massanalyse. Walter de Gruyter, Berlin
- Kästele X, Sturm C, Klüfers P (2014) ¹³C NMR spectroscopy as a tool for the in situ characterisation of iron-supplementing preparations. *Eur J Pharm Biopharm* 86:469–477
- Medice Pharma GmbH&Co. KG, Iserlohn, Germany (2011) MonoFer 100 mg/mL. Lösung zur Injektion und Infusion. <http://www.medice.de/produkte/nierenheilkunde/monofer>. Accessed 19 July 2013
- Klug HP, Alexander LE (1974) X-ray diffraction procedures. Wiley, New York
- Koskenkorva-Frank TS, Weiss G, Koppenol WH, Burckhardt S (2013) The complex interplay of iron metabolism, reactive oxygen and reactive nitrogen species: insights into the potential of different iron therapies to induce oxidative and nitrosative stress. *Free Radic Biol Med* 65:1174–1194
- Kudasheva S, Lai J, Ulman A, Cowman MK (2004) Structure of carbohydrate-bound polynuclear iron oxyhydroxide nanoparticles in parenteral formulations. *J Inorg Chem* 98:1757–1769
- Lippard SJ, Berg JM (1994) Principles of bioinorganic chemistry. University Science Books, Mill Valley
- Macdougall IC, Geisser P (2013) Use of intravenous iron supplementation in chronic kidney disease: an update. *Iran J Kidney Dis* 7:9–22
- Macdougall IC, Canaud B, de Francisco AL, Filippatos G, Ponikowski P, Silverberg D, van Veldhuisen DJ, Anker SD (2012) Beyond the cardiorenal anaemia syndrome: recognizing the role of iron deficiency. *Eur J Heart Fail* 14:882–886
- Mahmoudi L, Kissner R (2014) Electrode reactions of iron oxide-hydroxide colloids. *Dalton Trans* 43:15407–15413
- Merli D, Profumo A, Dossi C (2012) An analytical method for Fe(II) and Fe(III) determination in pharmaceutical grade iron sucrose complex and sodium ferric gluconate complex. *J Pharm Anal* 2:450–453
- Morup S, Tronc E (1994) Superparamagnetic relaxation of weakly interacting particles. *Phys Rev Lett* 72:3278–3281
- Munoz M, Martin-Montanez E (2012) Ferric carboxymaltose for the treatment of iron-deficiency anemia. *Expert Opin Pharmacother* 13:907–921 (corrected)
- Murad E (1996) Magnetic properties of microcrystalline iron(III) oxides and related materials as reflected in their Mössbauer spectra. *Phys Chem Miner* 23:248–262
- Murad E, Cashion J (2004) Mössbauer spectroscopy of environmental materials and their industrial utilization. Kluwer Academic Publishers, Boston

- Nordfjeld K, Andreassen H, Thomsen LL (2012) Pharmacokinetics of iron isomaltoside 1000 in patients with inflammatory bowel disease. *Drug Des Devel Ther* 6:43–51
- Pai AB, Garba AO (2012) Ferumoxytol: a silver lining in the treatment of anemia of chronic kidney disease or another dark cloud? *J Blood Med* 3:77–85
- Pawley GS (1981) Unit-cell refinement from powder diffraction scans. *J Appl Cryst* 14:357–361
- Pecharroman C, Gonzalez-Carreno T, Iglesias JE (1995) The infrared dielectric properties of maghemite, $\gamma\text{-Fe}_2\text{O}_3$, from reflectance measurement on pressed powders. *Phys Chem Miner* 22:21–29
- Pharmacosmos A/S, Holbaek, Denmark (2009) Public Assessment Report, Scientific discussion, MonoFer(R) 100 mg/mL solution for injection/infusion (iron(III)isomaltoside 1000). SE/H/734/01/DC, 2009. http://www.lakemedelsverket.se/SPC_PIL/Pdf/par/Monofer%20solution%20for%20infusion-injection.pdf. Accessed 22 March 2013
- Post JE, Buchwald VF (1991) Crystal structure refinement of akaganeite. *Am Miner* 76:272–277
- Qunibi WY (2010) The efficacy and safety of current intravenous iron preparations for the management of iron-deficiency anaemia: a review. *Arzneimittelforschung* 60:399–412
- Ravel B, Newville M (2005) ATHENA, ARTEMIS, HEPHAESTUS: data analysis for X-ray absorption spectroscopy using IFEFFIT. *J Synchrotron Radiat* 12:537–541
- Rosner MH, Auerbach M (2011) Ferumoxytol for the treatment of iron deficiency. *Expert Rev Hematol* 4:399–406
- Schellekens H, Stegemann S, Weinstein V, de Vlieger JS, Flühmann B, Mühlebach S, Gaspar R, Shah VP, Crommelin DJ (2014) How to regulate nonbiological complex drugs (NBCD) and their follow-on versions: points to consider. *AAPS J* 16:15–21
- Shander A, Van AH, Colomina MJ, Gombotz H, Hofmann A, Krauspe R, Lasocki S, Richards T, Slappendel R, Spahn DR (2012) Patient blood management in Europe. *Br J Anaesth* 109:55–68
- Simon GH, von Vopelius-Feldt J, Fu Y, Schlegel J, Pinotek G, Wendland MF, Chen MH, Daldrup-Link HE (2006) Ultrasmall superparamagnetic iron oxide-enhanced magnetic resonance imaging of antigen-induced arthritis: a comparative study between SHU 555 C, ferumoxtran-10, and ferumoxytol. *Invest Radiol* 41:45–51
- Steen DL, Cannon CP, Lele SS, Rajapurkar MM, Mukhopadhyay B, Scirica BM, Murphy SA, Morrow DA (2013) Prognostic evaluation of catalytic iron in patients with acute coronary syndromes. *Clin Cardiol* 36:139–145
- Stefansson BV, Haraldsson B, Nilsson U (2011) Acute oxidative stress following intravenous iron injection in patients on chronic hemodialysis: a comparison of iron-sucrose and iron-dextran. *Nephron Clin Pract* 118:c249–c256
- Toblli JE, Cao G, Oliveri L, Angerosa M (2012) Comparison of oxidative stress and inflammation induced by different intravenous iron sucrose similar preparations in a rat model. *Inflamm Allergy Drug Targets* 11:66–78
- Tronc E, Ezzir A, Cherkaoui R, Chanéac C, Noguès M, Kachkachi H, Fiorani D, Testa AM, Grenèche JM, Jolivet JP (2000) Surface-related properties of $[\gamma\text{-Fe}_2\text{O}_3]$ nanoparticles. *J Magn Magn Mater* 221:63–79
- Tucek J, Zboril R, Petridis D (2006) Maghemite nanoparticles by view of Mössbauer spectroscopy. *J Nanosci Nanotechnol* 6:926–947
- U.S. Food and Drug Administration (2012a) Draft guidance on iron sucrose. <http://www.fda.gov/downloads/Drugs/GuidanceComplianceRegulatoryInformation/Guidances/UCM297630.pdf>. Accessed 19 July 2013a
- U.S. Food and Drug Administration (2012b) Iron sucrose injection, official monograph. United States Pharmacopeial Convention, Rockville, pp 3564–3566
- U.S. Food and Drug Administration (2013) Draft guidance on sodium ferric gluconate complex. <http://www.fda.gov/downloads/Drugs/GuidanceComplianceRegulatoryInformation/Guidances/UCM358142.pdf>. Accessed 19 July 2013
- Van Wyck DB (2004) Labile iron: manifestations and clinical implications. *J Am Soc Nephrol* 15(Suppl 2):S107–S111
- Van Wyck DB, Anderson J, Johnson K (2004) Labile iron in parenteral iron formulations: a quantitative and comparative study. *Nephrol Dial Transpl* 19:561–565
- von Drygalski A, Adamson JW (2012) Iron metabolism in man. *JPEN* 37(5):599–606
- von Haehling S, Anker MS, Jankowska EA, Ponikowski P, Anker SD (2012) Anemia in chronic heart failure: can we treat? What to treat? *Heart Fail Rev* 17:203–210
- Woodcock J (2011) FDA/CDER to Chesapeake Regulatory Group, Inc., Frommer Lawrence and Haug LLP, and Covington & Burling LLP: Petition Partial Approval and Denial. <http://www.regulations.gov/#!documentDetail;D=FDA-2004-P-0494-0008>. Accessed 2 July 2013
- Young, RA (1993) Introduction to the Rietveld method. In: Young, RA (ed) *The Rietveld Method*, Oxford University Press, Oxford, pp IUCr book series
- Zager RA, Johnson AC, Hanson SY (2004) Parenteral iron therapy exacerbates experimental sepsis. *Kidney Int* 65:2108–2112